Electronic Supplementary Information (ESI)

One-dimensional van der Waals stacked p-type crystal $Ta_2Pt_3Se_8$ for nanoscale electronics

Byung Joo Jeong,‡[a] Kyung Hwan Choi,‡[b] Jiho Jeon,[b] Sang Ok Yoon,[a] You Kyoung Chung,[c] Dongchul Sung,[c] Sudong Chae,[a] Seungbae Oh,[a] Bum Jun Kim,[a] Sang Hoon Lee,[a] Chaeheon Woo,[a] Tae Yeong Kim,[a] Jungyoon Ahn,[a] Joonsuk Huh,[b,c,e] Jae-Hyun Lee,[d] Hak Ki Yu,*[d] and Jae-Young Choi*[a,b]

[a]*School of Advanced Materials Science & Engineering, Sungkyunkwan University, Suwon 16419, Republic of Korea*

[b]*SKKU Advanced Institute of Nanotechnology (SAINT), Sungkyunkwan University, Suwon 16419, Republic of Korea*

[c]*Department of Chemistry, Sungkyunkwan University, Suwon 16419, Republic of Korea*

[d]*Department of Materials Science and Engineering & Department of Energy Systems Research, Ajou University, Suwon 16499, Republic of Korea*

[e]*Institute of Quantum Biophysics, Sungkyunkwan University, Suwon 16419, Republic of Korea*

*To whom correspondence should be addressed. E-mail: jy.choi@skku.edu (J. Y. Choi), hakkiyu@ajou.ac.kr (H. K. Yu)

TABLE OF CONTENTS

Calculation of inter-ribbon binding energy

Supporting Figures

Fig. S1. Reaction temperature-dependent synthesis of $Ta_2Pt_3Se_8$ crystals

Fig. S2. XRD analysis of vapor-grown bulk $Ta_2Pt_3Se_8$ crystals

Fig. S3. EDS analysis of bulk $Ta_2Pt_3Se_8$ crystals

Fig. S4. Thermal stability of bulk $Ta_2Pt_3Se_8$ crystals

Fig. S5. Calculation of the electronic band structure of bulk $Ta_2Pt_3Se_8$.

Fig. S6. 7 nm-thick $Ta_2Pt_3Se_8$ FET

Fig. S7. Ti contact analysis

Fig. S8. Device stability analysis

Fig. S9. Modeling of Schottky barrier height

Fig. S10. P-N homogenous junction fabrication schematic

Fig. S11. P-N homogenous junction by partial encapsulation of Al_2O_3 layer

Calculation of inter-ribbon binding energy

To understand the structural dissociative property, we calculated the inter-ribbon bonding energy using the following formula:

$$E_b = -\left[E_{tot}(bulk) - \left\{2 \times E_{tot}(1D\ single\ ribbon)\right\}\right]/4$$

The molecular ribbons in bulk $Ta_2Pt_3Se_8$ have inter-ribbon bonding energy of 0.37 eV/atom, which is comparable to the binding energy of 0.24 eV/atom of hydrogen bond-type vdW forces between water molecules, as presented in Table S1. Therefore, we can expect that the weak vdW bonding between molecular ribbons provides the possibility of cleavage of bulk crystals into thinner nanoribbons by mechanical exfoliation. The following table shows the inter-ribbon bonding energy of bulk $Ta_2Pt_3Se_8$.

Reaction temperature-dependent synthesis of $Ta_2Pt_3Se_8$ crystals

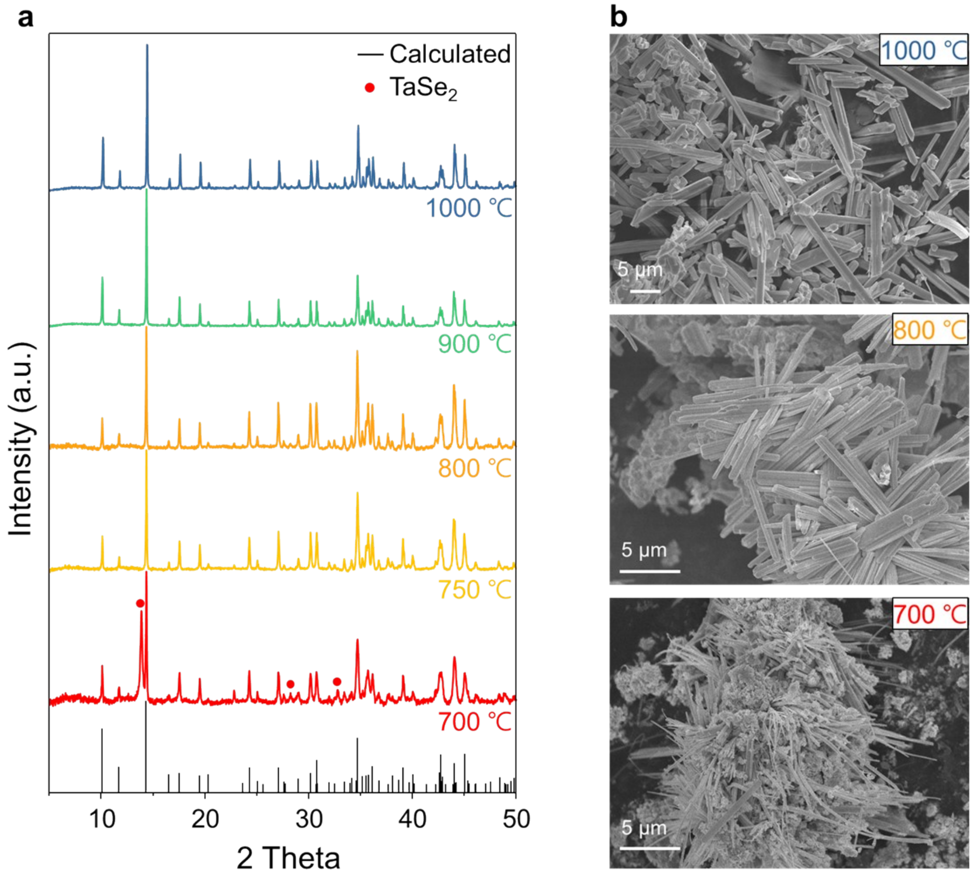

Fig. S1 Reaction temperature-dependent experiment at a stoichiometric composition (Ta: Pt: Se = 2: 3: 8). (a) XRD results of samples synthesized with an increase in temperature from 700 to 1000 °C. (b) SEM images of the synthesized samples with different reaction temperatures.

XRD analysis of vapor-grown bulk $Ta_2Pt_3Se_8$ crystals

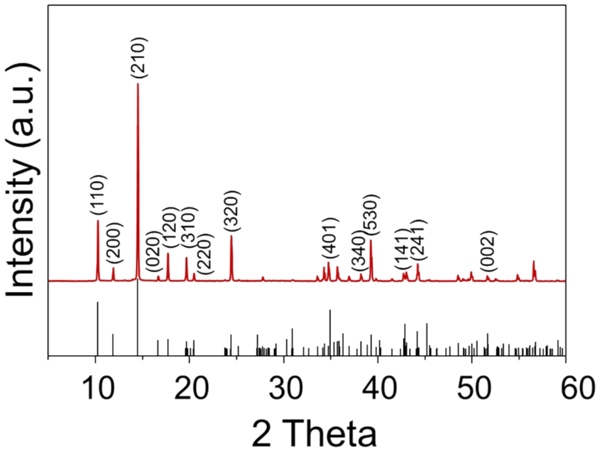

Fig. S2 XRD result of vapor-grown large $Ta_2Pt_3Se_8$ crystals synthesized at 1000 ℃ with Se excess condition (Ta: Pt: Se = 2: 3: 10). The samples obtained from this condition were used in further characterization and device fabrication.

EDS analysis of bulk $Ta_2Pt_3Se_8$ crystals

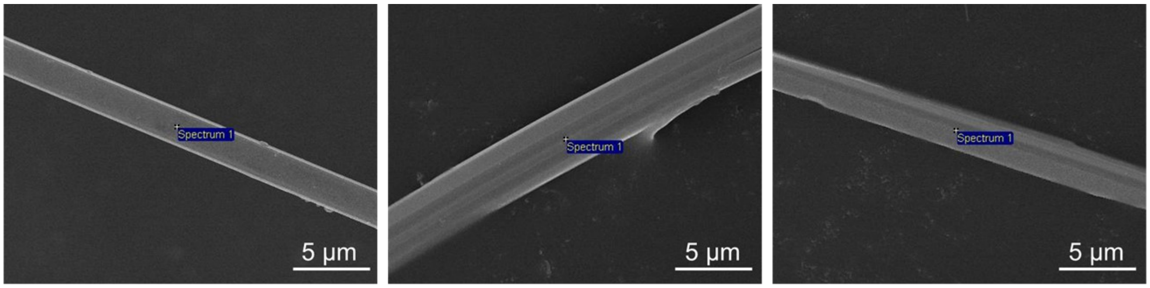

Element	Weight%	Atomic%
Ta M	22.38	15.54
Pt M	41.22	26.54
Se L	36.41	57.92
Totals	100	

Element	Weight%	Atomic%
Ta M	23.40	16.36
Pt M	41.01	26.59
Se L	35.60	57.04
Totals	100	

Element	Weight%	Atomic%
Ta M	24.19	16.99
Pt M	40.74	26.55
Se L	35.07	56.46
Totals	100	

Fig. S3 EDS data of the bulk $Ta_2Pt_3Se_8$ crystals on multiple positions at different locations of the sample, representing atomic percent close to Ta: Pt: Se = 2: 3: 8.

Thermal stability of bulk $Ta_2Pt_3Se_8$ crystals

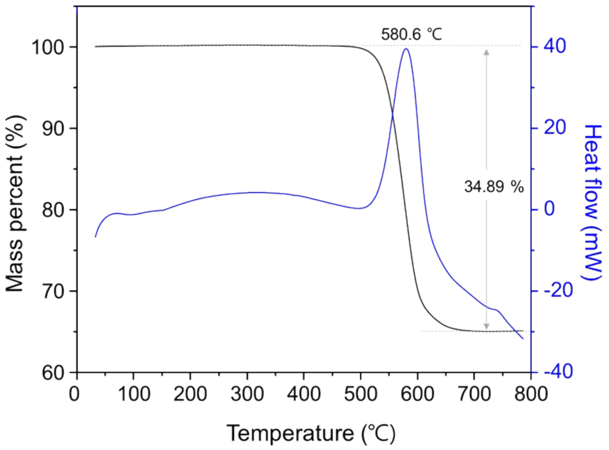

Fig. S4 TG-DSC measurement of bulk $Ta_2Pt_3Se_8$ crystals

Calculation of the electronic band structure of bulk $Ta_2Pt_3Se_8$

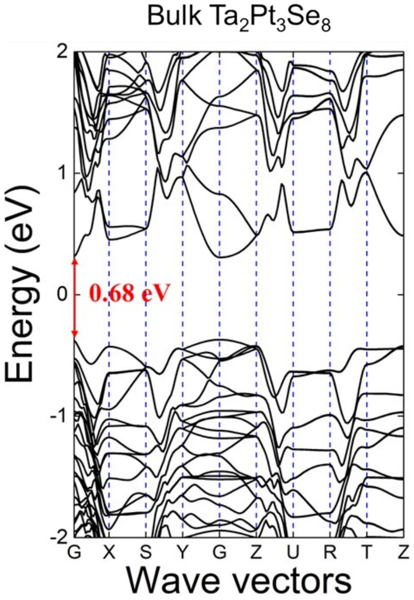

Fig. S5 Calculated electronic band structure of bulk $Ta_2Pt_3Se_8$.

7 nm-thick $Ta_2Pt_3Se_8$ FET

The work function of $Ta_2Pt_3Se_8$ gradually decreased as the thickness of $Ta_2Pt_3Se_8$ decreased. In the field-effect measurement of 7 nm thick $Ta_2Pt_3Se_8$ nanoribbon, we observed a slight Schottky behavior in the I-V curve and a typical p-type characteristic in the transfer curve. The extracted mobility was recorded as 1.6 $cm^2\ V^{-1}s^{-1}$ at V_{ds} of 1 V, and the I_{on}/I_{off} ratio exceeded 10^4.

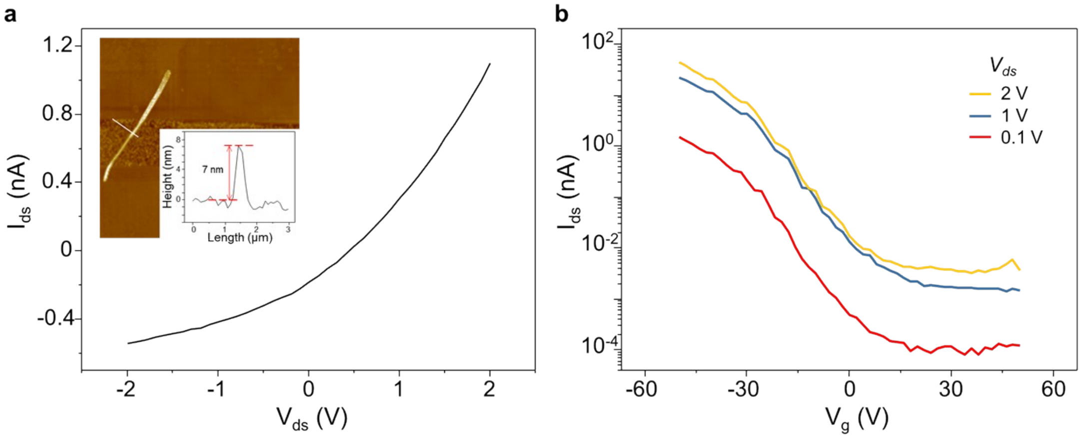

Fig. S6 7 nm-thick $Ta_2Pt_3Se_8$ FET electrical characteristics. (a) I-V curve of 7 nm-thick $Ta_2Pt_3Se_8$. Inset shows AFM image with its height profile. (b) P-type transfer characteristic of 7 nm-thick $Ta_2Pt_3Se_8$ at RT.

Ti contact analysis

We tested the field-effect characteristics of several multilayer $Ta_2Pt_3Se_8$ FETs using Ti/Au (20 nm / 60 nm) as electrodes. The output curve of $Ta_2Pt_3Se_8$ showed a Schottky contact at all gate biases. In addition, the transfer curves of each device indicated that the I_{on}/I_{off} ratio and current level were significantly degraded compared to the previous results, that is, transfer curves using Ni/Au electrodes. Therefore, it is plausible that the Ti/Au electrode creates a high Schottky barrier with $Ta_2Pt_3Se_8$ owing to its low work function.

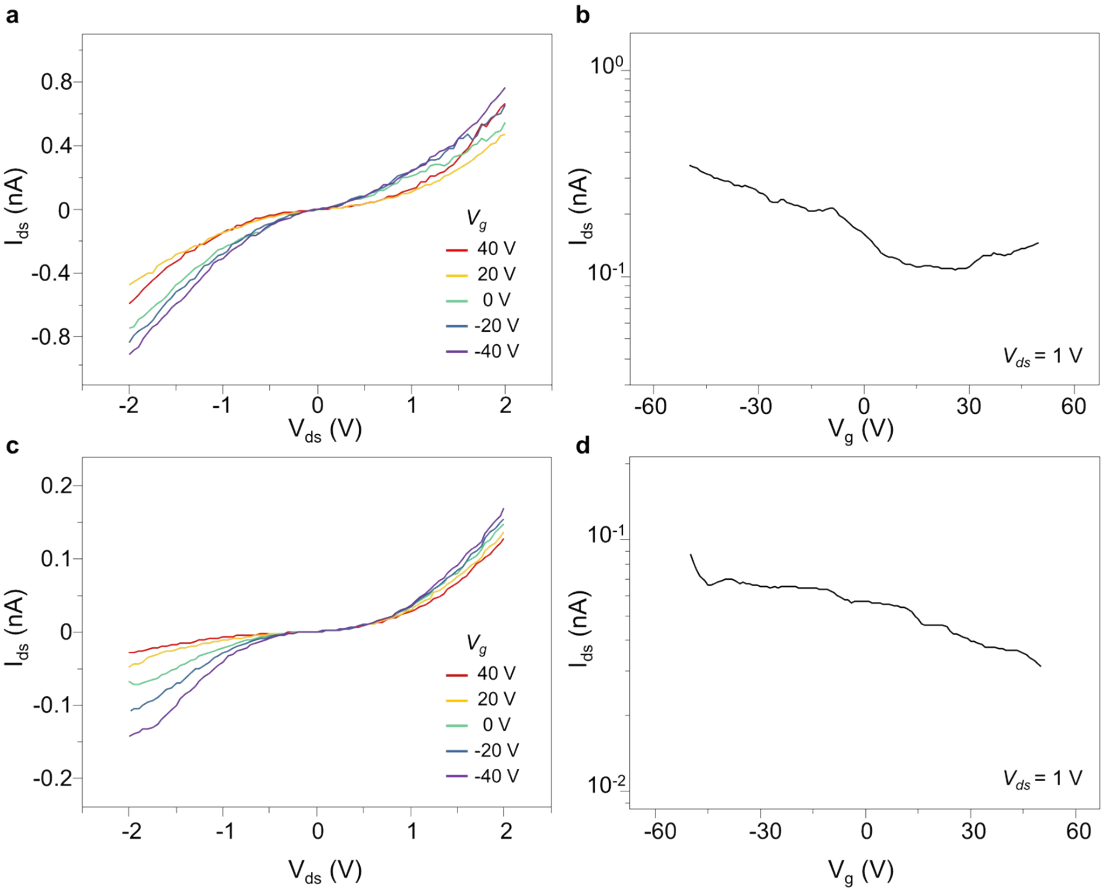

Fig. S7 Ti contact $Ta_2Pt_3Se_{8\ \mathrm{FET}}$ characteristic. (a) 28 nm-thick $Ta_2Pt_3Se_8$ output characteristic at different gate biases and (b) transfer characteristic at RT. (c) 16 nm-thick $Ta_2Pt_3Se_8$ output characteristic at different gate biases and (d) transfer characteristic at RT.

Device stability analysis

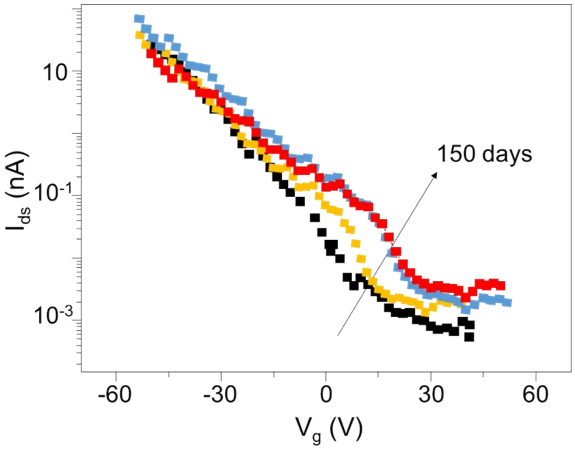

Fig. S8 Stable p-type transfer characteristic of $Ta_2Pt_3Se_8$ FET

Modeling of Schottky barrier heights

Generally, to extract the formula for the Schottky barrier height, a thermionic emission current model was used to explain the charge barrier overcame between the metal and the semiconductor through a quantum-mechanical process. When V_{ds} is applied to the device, the potential barrier to be overcome by electrons is $\Phi_{SB} - V_{ds}$ (Φ_{SB} is a notation of Schottky barrier height). A generalization for n-dimensional materials considering an (n-1) dimension surface in k-space, the current density is given by

$$J_n = R_n T^{(n+1)/2} \exp\left(\frac{-q(\Phi_B - V_{ds})}{k_B T}\right) \qquad (1)$$

where n is n-dimension.[1] The Richardson constant is given by:

$$R_n^* = 2^{(n+1)/2}\, \pi^{(n-1)/2} m^{(n-1)/2} k_B^{(n+1/2)} h^{-n} q \qquad (2)$$

Therefore, in 2D, the temperature term in the prefactor changes to $T^{3/2}$ and in 1D as T. Through equation 2, we can derive the 2D and 1D thermionic emission equation:

2D thermionic emission:

$$I_{2D} = A_c R_{2D}^* T^{3/2} \exp\left[\frac{-q(\Phi_{SB})}{k_B T}\right]\left[\exp\left(\frac{qV_{ds}}{k_B T}\right)\right], \quad R_{2D}^* = \frac{q(8\pi m^* k_B^3)^{1/2}}{h^2} \qquad (3)$$

1D thermionic emission:

$$I_{1D} = A_c R_{1D}^{*} T \exp\left[\frac{-q(\Phi_{SB})}{k_B T}\right]\left[\exp\left(\frac{qV_{ds}}{k_B T}\right)\right], \qquad R_{1D}^{*} = \frac{2qk_B}{h} \tag{4}$$

where A_c is the contact area, R^* is the Richardson constant, k_B is the Boltzmann constant, and if $Ta_2Pt_3Se_8$ is considered as a 1-dimension material, the 2D model could be adjusted to explain its transport mechanism such that the SBH was extracted using log $(I/T^{3/2})$ as a function of the 1/T plot. As shown in Fig. S8 each SBH of the hole extracted from the two models shows almost the same value as the difference of SBH_{hole} 21 meV.

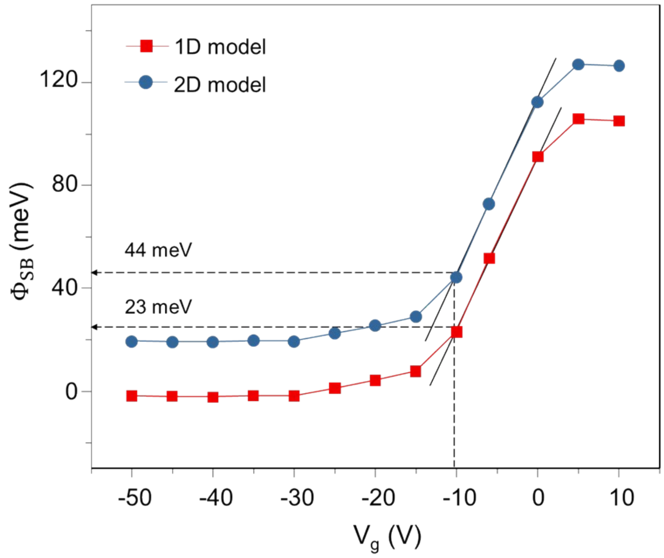

Fig. S9. Modeling of Schottky barrier heights.

P-N homogenous junction fabrication schematic

Before the formation of a partially encapsulated device structure to show the P-N diode characteristics, we made source-drain contact to $Ta_2Pt_3Se_8$ using a TEM grid. Subsequently, the atomic layer deposition process of the Al_2O_3 layer was performed. Next, using a typical photolithography method, a photoresist pattern was placed on the $Ta_2Pt_3Se_8$ nanoribbon with only half of the wire covered. To form a partially encapsulated device, the air-exposed Al_2O_3 layer was etched by a 6:1 buffered oxide etchant bath for 5 s. Finally, the electron beam was irradiated onto the device with one electrode grounded to the metal holder during the e-beam doping process.

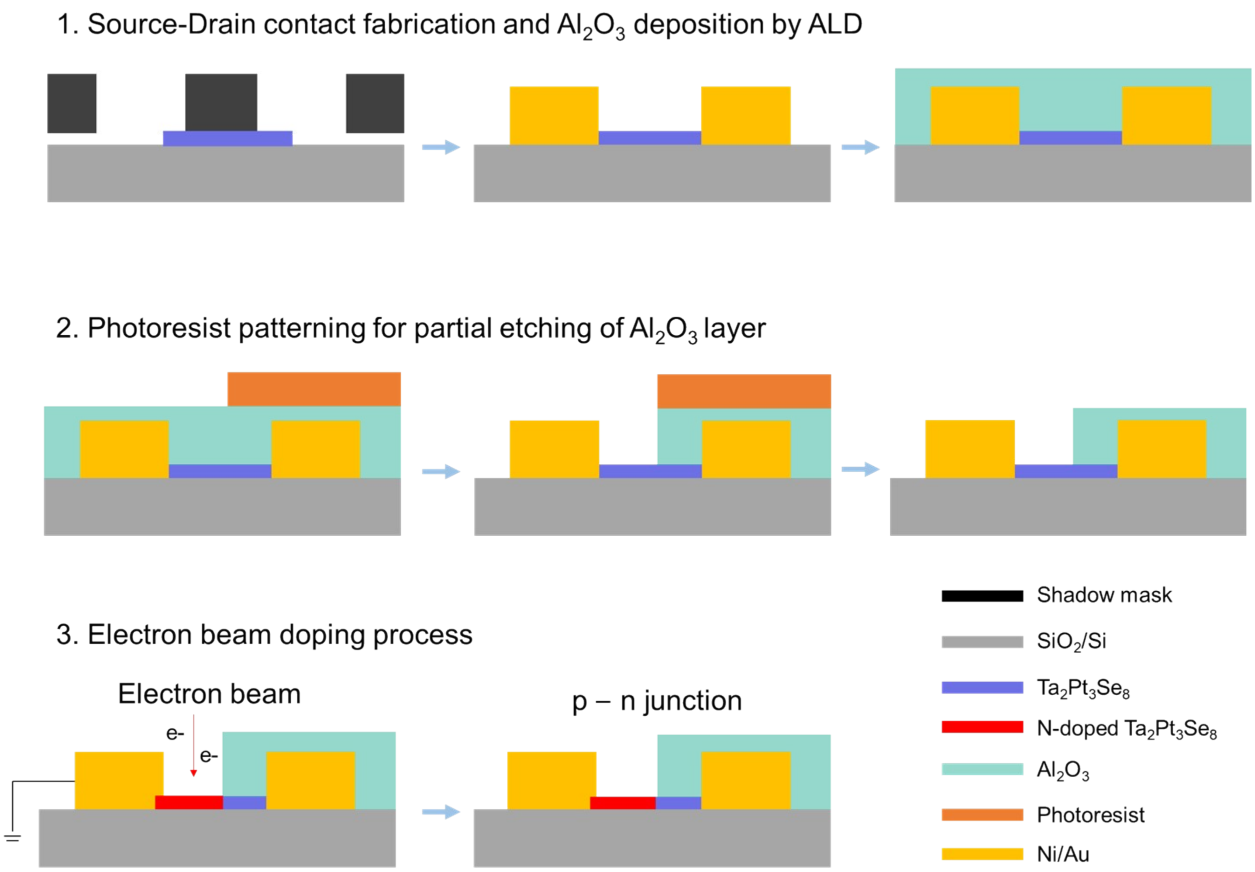
1. Source-Drain contact fabrication and Al_2O_3 deposition by ALD

2. Photoresist patterning for partial etching of Al_2O_3 layer

3. Electron beam doping process

Fig. S10 $Ta_2Pt_3Se_8$ homogenous p-n junction device fabrication schematic using the electron beam doping method.

P-N homogenous junction by partial encapsulation of Al_2O_3 layer

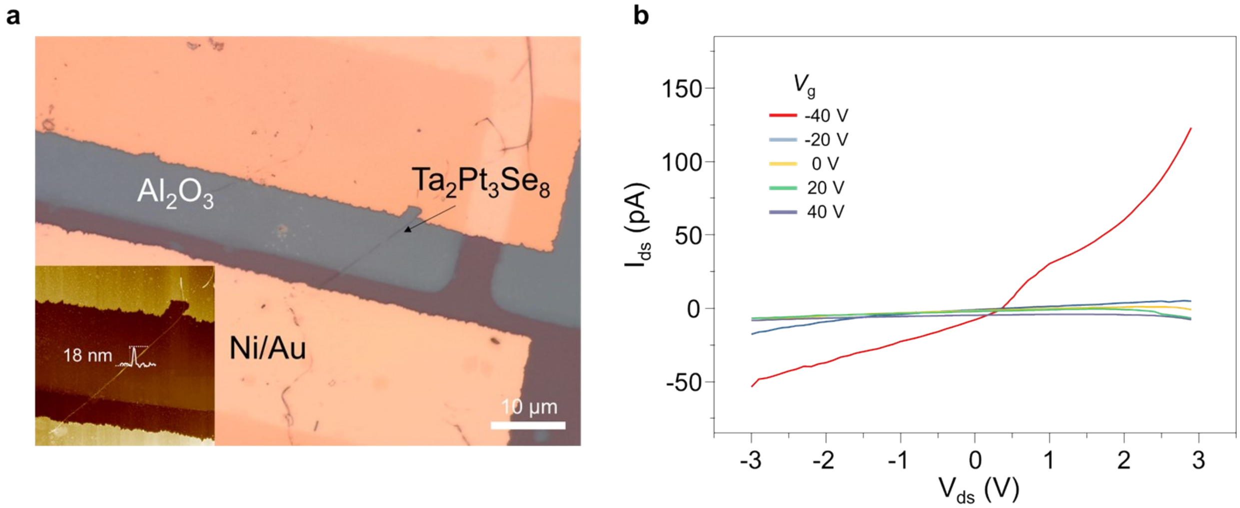

Fig. S11 Device structure and diode performance. (a) Optical microscopy images of partial Al_2O_3 layer encapsulation structure for p-n homogenous junction $Ta_2Pt_3Se_8$. The inset shows the AFM image of device and $Ta_2Pt_3Se_8$ thickness of 18-nm. (b) Diode performance of $Ta_2Pt_3Se_8$.

REFERENCES

(1) M. F. O'Dwyer, R. A. Lewis, C. J. Zhang, *Microelectronics J*. 2008, **39**, 597-600.